Developmental Cell
Article

The N-Myc-DLL3 Cascade Is Suppressed by the Ubiquitin Ligase Huwe1 to Inhibit Proliferation and Promote Neurogenesis in the Developing Brain

Xudong Zhao,[1,9] Domenico D' Arca,[1,9] Wei Keat Lim,[2,3,10] Manisha Brahmachary,[3] Maria Stella Carro,[1] Thomas Ludwig,[1,4] Carlos Cordon Cardo,[4] Francois Guillemot,[5] Ken Aldape,[6] Andrea Califano,[2,3] Antonio Iavarone,[1,4,7,*] and Anna Lasorella[1,4,8,*]

[1]Institute for Cancer Genetics
[2]Department of Biomedical Informatics
[3]Center for Computational Biology and Bioinformatics
[4]Department of Pathology
Columbia University Medical Center, New York, NY 10032, USA
[5]Division of Molecular Neurobiology, National Institute for Medical Research, The Ridgeway, Mill Hill, London NW7 1AA, UK
[6]Department of Pathology, M.D. Anderson Cancer Center, Houston, TX 77030, USA
[7]Department of Neurology
[8]Department of Pediatrics
Columbia University Medical Center, New York, NY 10032, USA
[9]These authors contributed equally to this work
[10]Present address: Therasis Inc., Bellevue Hospital Center, 462 First Avenue, Suite 908, New York, NY 10016, USA
*Correspondence: ai2102@columbia.edu (A.I.), al2179@columbia.edu (A.L.)
DOI 10.1016/j.devcel.2009.07.009

SUMMARY

Self-renewal and proliferation of neural stem cells and the decision to initiate neurogenesis are crucial events directing brain development. Here we show that the ubiquitin ligase Huwe1 operates upstream of the N-Myc-DLL3-Notch pathway to control neural stem cell activity and promote neurogenesis. Conditional inactivation of the *Huwe1* gene in the mouse brain caused neonatal lethality associated with disorganization of the laminar patterning of the cortex. These defects stemmed from severe impairment of neurogenesis associated with uncontrolled expansion of the neural stem cell compartment. Loss- and gain-of-function experiments in the mouse cortex demonstrated that Huwe1 restrains proliferation and enables neuronal differentiation by suppressing the N-Myc-DLL3 cascade. Notably, human high-grade gliomas carry focal hemizygous deletions of the X-linked *Huwe1* gene in association with amplification of the *N-myc* locus. Our results indicate that Huwe1 balances proliferation and neurogenesis in the developing brain and that this pathway is subverted in malignant brain tumors.

INTRODUCTION

During development of mammalian neocortex, generation of neurons (neurogenesis) is preceded by proliferation of neural stem cells and committed progenitors in the germinal compartments lining the cerebral ventricles—the ventricular zone (VZ) and the subventricular zone (SVZ) (Doe, 2008; Gotz and Huttner, 2005). Neocortical neurogenesis in the VZ of the normal mouse extends from E11 through E18 (Takahashi et al., 1993, 1994, 1995a, 1995b). During this time the cell cycle length increases, the proliferating fraction of neuroepithelial progenitors in the VZ gradually decreases, and the fraction of cells exiting the cell cycle and undergoing differentiation progressively increases (Dehay and Kennedy, 2007; Gotz and Huttner, 2005; Takahashi et al., 1995a, 1995b). The increasing fraction of progenitors withdrawing from the cell cycle is paralleled by activation of differentiation programs for the neuronal lineage, thus ensuring that the correct number of neuronal subtypes are consistently generated and form the functional circuits that orchestrate the laminar organization of the cortex (Kintner, 2002). Protein ubiquitination has recently emerged as a rapid and efficient posttranslational modification of substrates that regulates many biological conditions. Specificity for distinct substrates is conferred by the E3 ubiquitin ligase subunit. When ubiquitin tagging to intracellular substrates occurs through Lys48-linked polyubiquitin chains, proteins are labeled for 26S proteasome-mediated recognition and proteolytic destruction. Little is known about the nature and dynamics of E3 ubiquitin ligases that, in response to antimitogenic and differentiative signals, modify key transcriptional regulators to instigate the transition from dividing neural progenitors to postmitotic neurons.

Huwe1 encodes a HECT domain ubiquitin ligase. Through covalent interactions with the catalytic cysteine residue, HECT domain ligases accept ubiquitin from E2 ubiquitin-conjugating enzymes and transfer the ubiquitin to specific substrates (Huang et al., 1999). Huwe1 is a large protein (~500 kD) that has attracted considerable interest because several and quite disparate substrates have been assigned to this E3 (histones, Mcl1, p53, c-Myc, cdc6, N-Myc) (Adhikary et al., 2005; Chen et al., 2005; Hall et al., 2007; Liu et al., 2005; Zhao et al., 2008; Zhong et al., 2005). Not surprisingly, the biological functions of Huwe1 remain controversial (Bernassola et al., 2008). We have generated mice in which the region coding for the HECT domain of

Huwe1 has been floxed. Targeted inactivation of floxed *Huwe1* in the mouse brain disclosed that Huwe1-mediated ubiquitination is essential to restrain proliferation, elicit neurogenesis, and establish the laminar structure of the cortex. This activity is abolished in malignant brain tumors containing genetic or epigenetic inactivation of *Huwe1*.

RESULTS

Targeted Inactivation of Huwe1 in the CNS Results in Neonatal Lethality

The pattern of expression of the Huwe1 protein in the nervous system is characterized by an increasing gradient, with the lowest amounts in the regions that contain neural stem cells/undifferentiated progenitors (VZ/SVZ) and the highest levels in differentiated neurons (cortical plate [CP]) (Zhao et al., 2008). To determine the requirement for Huwe1 during development of the nervous system, we used a conditional *Huwe1* mutant allele in which exon 80 and exon 82, which encode the HECT domain of the Huwe1 protein, were flanked by LoxP sites (Zhao et al., 2008). To inactivate *Huwe1*, we used a *Cre* deleter strain that was driven by the Nestin promoter, resulting in expression throughout the nervous systems from E10.5 (Lothian et al., 1999). *Huwe1* gene is X-linked, thus we performed our analysis on male offspring because inactivation of the single *Huwe1* allele in this gender results in the *Huwe1* null genotype (see Figure S1A available online). Crossings between $Huwe1^{Flox/X}$ or $Huwe1^{Flox/Flox}$ females and *Nestin-Cre* transgenic males generated $Huwe1^{Flox/Y}$*Nestin-Cre* animals (hereafter referred to as $Huwe1^{F/Y}$*Nes*). We observed efficient deletion of *Huwe1* in the nervous system (Figures S1A and S1B). Western blot and immunofluorescence analysis of Huwe1 protein using two antibodies recognizing the N terminus (Huwe1 N-ter) or the HECT domain at the C terminus (Huwe1 HECT) confirmed that the HECT domain was absent in the brain of $Huwe1^{F/Y}$*Nes* pups. Moreover, the mutant Huwe1 protein was markedly reduced, suggesting that C-terminal deletion destabilized the residual polypeptide (Figures S1C and S1D). $Huwe1^{F/Y}$*Nes* mice were born with the expected ratio. However, all $Huwe1^{F/Y}$*Nes* neonates died within 24 hr of postnatal life (Table S1 available online).

Deletion of Huwe1 Deregulates Proliferation and Impairs Cell Cycle Withdrawal and Lengthening of Cell Cycle Timing of Cortical Progenitors

The brains from $Huwe1^{F/Y}$*Nes* newborns were slightly smaller than those from $Huwe1^{F/Y}$ or $Huwe1^{+/Y}$*Nes* and wild-type littermates. Histologic analysis of the mutant brains at E18.5 and P0 revealed distinct abnormalities in various regions of the brain, including cerebral cortex, hippocampus, and cerebellum (Figures S2A, S2E, and S2F). Mutant mice had a poorly developed dentate gyrus and an immature, very small cerebellum (Figures S2E and S2F). In $Huwe1^{F/Y}$*Nes* mice cortical thickness was significantly reduced, the laminar organization was altered, and superficial neuron layers were not clearly identifiable (Figure S2C). Conversely, the germinal layers (VZ/SVZ) that contain proliferating neural stem/progenitor cells were expanded and extended into regions normally occupied by differentiating cells. Despite the overall reduction in cortical size, cellular density throughout the cortex was increased and intervening neuropil decreased (Figures S2A and S2C). Furthermore, mutant brains contained ectopic cellular clusters in differentiated striatal regions or, more rarely, other postmitotic areas of the brain (Figures S2B and S2D). At E15.5 histology abnormalities were barely discernible in mutant brains.

The increased cellular density in the neonatal cortex suggested that neuronal production was abnormal. To study cell proliferation, we performed quantitative analysis of the proliferation marker Ki67 at different embryonic stages (E13.5, E15.5, and E18.5). At each stage of development *Huwe1* knockout cortices contained significantly higher numbers of proliferating cells (Figures 1A, S3A, and S3B). Germinal areas (VZ and SVZ) were primarily involved in the proliferative expansion. However, the ectopic clusters dispersed throughout postmitotic and differentiated regions of the *Huwe1* knockout brain were also invariably positive to Ki67 (Figure 1B). Therefore, loss of Huwe1 deregulates the growth control in the nervous system and causes expansion of the germinal layers and ectopic clustering of proliferating cells. Also the higher number of Ki67-positive cells in $Huwe1^{F/Y}$*Nes* E13.5 and E15.5 embryos indicated that hyperproliferation precedes cortical abnormalities in *Huwe1* null brains.

Cortical neurogenesis is associated with progressive lengthening of the cell cycle and results in increased fraction of progenitors that exit the cell cycle and differentiate (Dehay and Kennedy, 2007; Gotz and Huttner, 2005). We asked whether the expansion of the neural progenitor pool in $Huwe1^{F/Y}$*Nes* animals is consequent to defective withdrawal and/or shortening of the cell cycle in comparison with normal brains. We analyzed the probability to withdraw from cycling and the cell cycle timing in $Huwe1^{F/Y}$*Nes* and wild-type embryos. First, we determined the fraction of cells that exit cell cycle after 24 hr labeling with bromodeoxyuridine (BrdU). The cell cycle exit was estimated as the fraction of BrdU-positive cells that lost positivity for Ki67 ($BrdU^{+}/Ki67^{-}$) and the total number of BrdU-positive cells. Quantification of these experiments from multiple pairs of *Huwe1* null and control brains at E13.5, E15.5, and E18.5 demonstrated that the fraction of progenitors that exited cell cycle was significantly lower in *Huwe1* null brains at each developmental age (Figures 1C, S3C, and S3D). To unravel potential changes in cell cycle timing, we determined the proportion of cortical progenitors labeled by 1 hr pulse BrdU, whereby neural progenitor cells are identified by Ki67 staining. Because the length of S phase remains constant throughout development, a larger fraction of BrdU-positive neural progenitors (Ki67-positive) would indicate shortening of the cell cycle, whereas a lower proportion would imply a prolonged cell cycle timing. Quantification of results from three pairs of control and *Huwe1* null brains indicated that the length of the cell cycle of the mutants was indistinguishable from that of the wild-type brains at E13.5 and E15.5 (Figures S4A and S4B). However, when the same analysis was conducted at E18.5, *Huwe1* null brains contained a significantly higher fraction of BrdU-positive progenitors, thus indicating that loss of Huwe1 shortened cell cycle timing at the latest stages of neural development (Figure 1D). Taken together, cell cycle withdrawal and timing analyses suggest that the primary defect caused by loss of Huwe1 is the reduced probability to exit from active cycling. However, as development proceeds, *Huwe1* inactivation impairs also the lengthening of cell cycle timing, which is normally

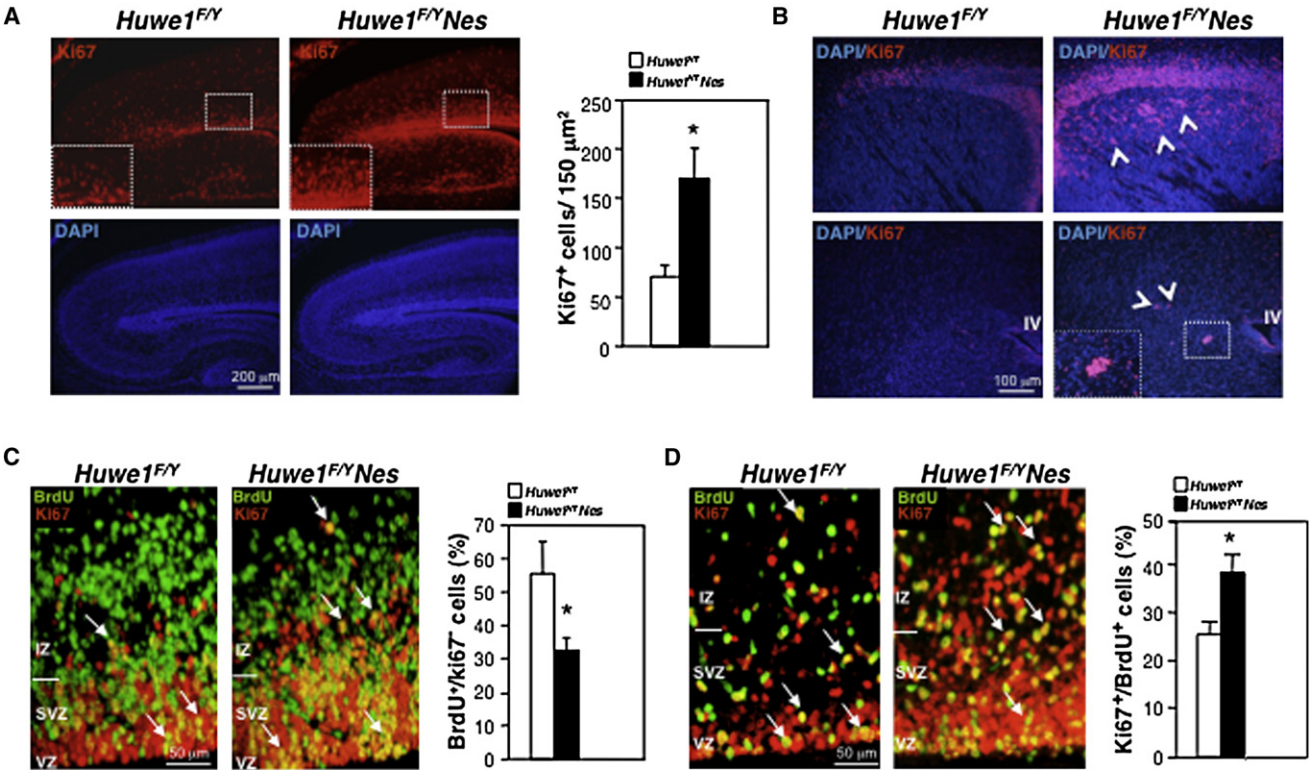

Figure 1. Deletion of the HECT Domain of *Huwe1* in the Brain Increases the Size of the Progenitor Pool and Alters Cell Cycle

(A) Sagittal sections of the cortex of embryos at E18.5 were stained for Ki67 (upper panels) and counterstained with DAPI (lower panels). Quantification of $Ki67^+$ cells normalized by area (150 μm^2) is shown in the graph. Bars indicate mean ± SD; n = 3 for $Huwe1^{F/Y}$ and 3 for $Huwe1^{F/Y}Nes$; p = 0.0008.

(B) Cortical sections at E18.5 were stained for Ki67 (red) and counterstained with DAPI (blue). Clusters of $Ki67^+$ cells are detected in $Huwe1^{F/Y}Nes$ basal ganglia (upper panel) and mesencephalic area (lower panel). Arrowheads indicate $Ki67^+$ clusters of cells. IV, IV ventricle.

(C) Immunofluorescence for Ki67 (red) and BrdU (green) 24 hr after a single pulse of BrdU in E15.5 embryos. The fraction of cells labeled only with BrdU ($BrdU^+/Ki67^-$, no longer dividing), as compared with $BrdU^+/Ki67^+$ cells (re-entering cell cycle), was scored. Bars indicate mean ± SD; n = 3 for $Huwe1^{F/Y}$ and 3 for $Huwe1^{F/Y}Nes$; p = 0.016.

(D) Immunofluorescence for Ki67 (red) and BrdU (green) after 1 hr pulse of BrdU in E18.5 embryos. The fraction of cycling progenitor cells ($Ki67^+$) labeled with BrdU was scored. Bars indicate mean ± SD; n = 3 for $Huwe1^{F/Y}$ and 3 for $Huwe1^{F/Y}Nes$; p = 0.006. Arrows indicate $BrdU^+/Ki67^+$.

associated with the increased rate of progenitors undergoing differentiation during late neurogenesis.

Perturbation of Differentiation and Disruption of Cortical Layering in the *Huwe1* Null Brain

We determined whether the ability to differentiate was also perturbed in *Huwe1* null brains. The RNA binding protein HuC/D is an early marker of neuronal differentiation expressed in the developing cortical plate since the initial stages of neurogenesis. It functions to promote neuronal differentiation by modulating the expression of genes required for axonal outgrowth such as the gene encoding for the GAP43 protein (Ekstrom and Johansson, 2003). HuC/D and GAP43 were readily detected in wild-type cortices at E15.5, but the expression of the two markers was notably reduced in $Huwe1^{F/Y}Nes$ brains (Figure 2A). GAP43 was also diminished in the mutant cortex at E18.5 (Figure S5A). The developmental progression from a neuroepithelial progenitor/radial glia phenotype, characteristic of the VZ, to an intermediate progenitor phenotype, predominant in the SVZ, is accompanied by downregulation of the homeodomain transcription factor Pax6 and concomitant induction of the T-box transcription factor Tbr2 (Englund et al., 2005). We compared the size and spatial distribution of these populations between the $Huwe1^{F/Y}Nes$ and control brains at E18.5. In wild-type cortex Pax6 was confined to the thin VZ layer and Tbr2 was detected as a more superficial domain coinciding with the SVZ. Conversely, *Huwe1* null cortex exhibited expansion and increased cellular density of the Pax6 expressing domain with consequent superficial displacement of the Tbr2-positive region. The thickness of the Tbr2 domain was similar among wild-type and *Huwe1* null cortices (Figure 2B, see also Figure S5B for P0). These findings indicate that loss of Huwe1 in the cortex induces uncontrolled growth of the Pax6-expressing stem/progenitor population, which remains negative for Tbr2. Next, we used molecular markers to determine the consequences of genetic inactivation of *Huwe1* on laminar structure of the cortex. In the normal brain the transcription factor Tbr1 and the Ctip2 protein are expressed in the deep cortical layers and mark early-born neurons. As late-born neurons populate the upper layers of the cortex, more superficial layers positive for MAP2, Cux1, and $p27^{Kip2}$ (layers II–III) juxtapose the Tbr1/Ctip2-expressing domains. Staining for Tbr1 and Ctip2 demonstrated decreased thickness but

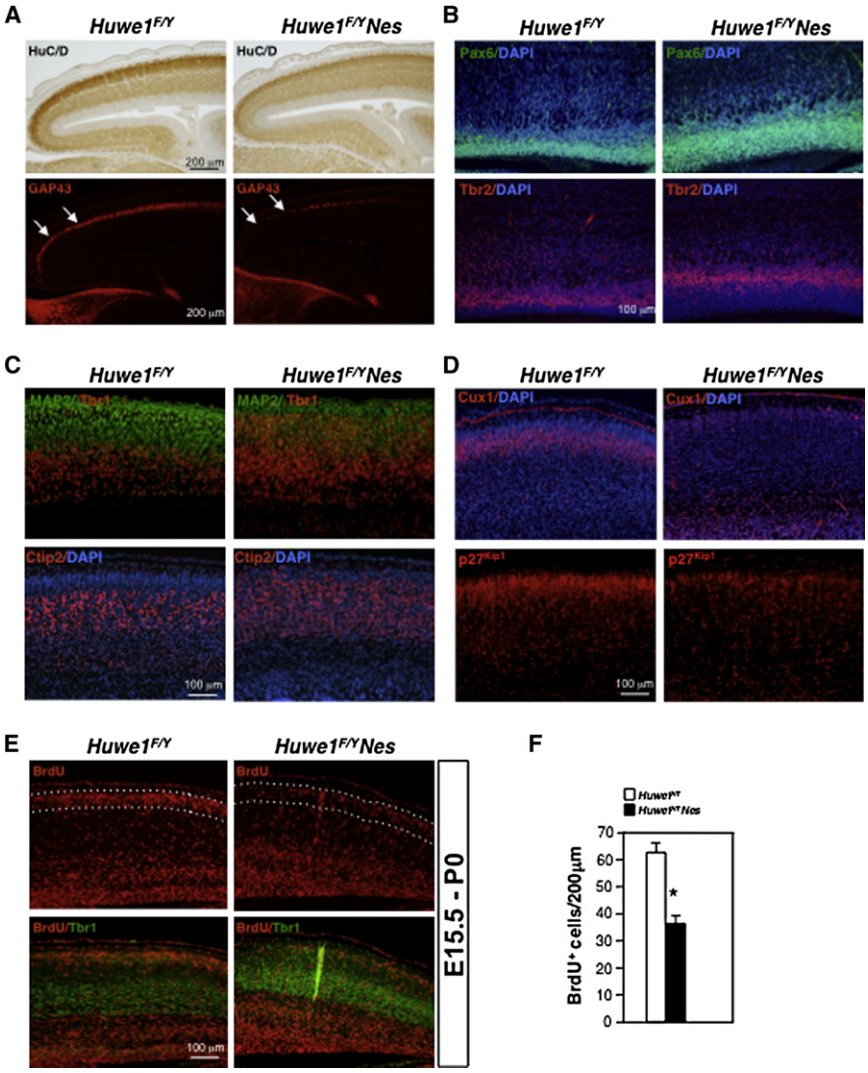

Figure 2. Defective Cortical Differentiation, Lamination, and Neurogenesis in *Huwe1*$^{F/Y}$*Nes* Embryos

(A) Sagittal sections of the cortex of embryos at E15.5 stained for HuC/D (upper panel) and GAP43 (lower panel). Arrows point to regions in which GAP43 expression is reduced.

(B) Staining for Pax6 (green, upper panels) and Tbr2 (red, lower panels) in E18.5 brains. Nuclei were counterstained with DAPI (blue). Note the expansion of the Pax6 domain with superficial displacement of the Tbr2^{+} region in the *Huwe1* null cortex.

(C) Immunofluorescence for MAP2 (green), Tbr1 (red) (upper panels), and Ctip2 (lower panels) in E18.5 cortices. Nuclei were counterstained with DAPI (blue).

(D) Staining for Cux1 (upper panels) and p27^{Kip1} (lower panels) in E18.5 cortices. Nuclei were counterstained with DAPI (blue).

(E) Immunofluorescence for BrdU (red) and Tbr1 (green) on cortical sections of P0 pups after injection of BrdU at E15.5.

(F) Quantification of BrdU^{+} neurons in the superficial layers (II–III) marked by dashed lines in (E). Bars indicate mean ± SD; n = 4 for *Huwe1*$^{F/Y}$ and 4 for *Huwe1*$^{F/Y}$*Nes*; p = 0.0005.

increased neuron packing density of the Tbr1/Ctip2-positive deep layers in *Huwe1*$^{F/Y}$*Nes* embryos and neonates (Figures 2C and S5C). Moreover, the most superficial layers of the cortical plate of *Huwe1* null embryos (layers II–III), marked by expression of MAP2, Cux1, and p27^{Kip2}, reached only a rudimentary development, being mostly occupied by a disordered population of Tbr1/Ctip2-positive neurons (Figures 2C, 2D, and S5C). To examine the efficiency of neuronal production and explore the mechanisms that lead to perturbed lamination in the *Huwe1*$^{F/Y}$*Nes* brain, we determined the position of neurons that became postmitotic at different times using the BrdU "birthdating" method. To examine early neurogenesis (deep layer neurons), BrdU was given to pregnant females when their embryos were at E12.5. To examine late neurogenesis (superficial layers), BrdU was given at E15.5; in both cases brains were dissected at P0. BrdU labeling at E12.5 showed no major defect in the position and absolute number of deep layer Tbr1-positive neurons (Figure S6A and S6B). However, a differentiation defect was already evident at this stage because mutant brains contained a significantly lower fraction of BrdU-positive neurons that stained positive for Tbr1 (Figure S6B, right panel). We interpret these findings to indicate that, although the percentage of progenitors undergoing differentiation is reduced in the *Huwe1* null cortex, the larger pool of progenitors available in the knockout brain accounts for a comparable number of Tbr1-positive neurons in layer VI. BrdU labeling at E15.5 indicated that the ability to generate neurons that migrate to the most superficial layers was markedly reduced in the absence of Huwe1 (Figures 2E and 2F). The observation that the *Huwe1* null brain displays normal staining pattern for Reelin, a key regulator of radial migration (Figure S6C), suggests that the increased neuron packing density in the mutant cortex is not secondary to cell-intrinsic migration defects. In sum, Huwe1 directs differentiation in the developing mouse cortex and is essential for the neuronal differentiation events that accompany the generation of late-born neurons in layers II–III.

The Expression Level of Huwe1 Controls Activation of a Neural-Specific N-Myc Regulon

To identify the mechanistic basis of the *Huwe1* knockout phenotype, we asked whether loss of *Huwe1* resulted in accumulation of N-Myc and uncontrolled activation of molecular events downstream of N-Myc. Immunostaining of control and *Huwe1* knockout brain revealed that N-Myc was elevated at E13.5, E15.5, and E18.5 (Figure 3A, upper panels, and Figures S7A and S7B, upper panels). D-type cyclins are established N-Myc target genes and are expressed in the developing CNS (Glickstein et al., 2007; Oliver et al., 2003). As for N-Myc, cyclin D1 was also weakly expressed throughout the cortical layers of wild-type embryos,

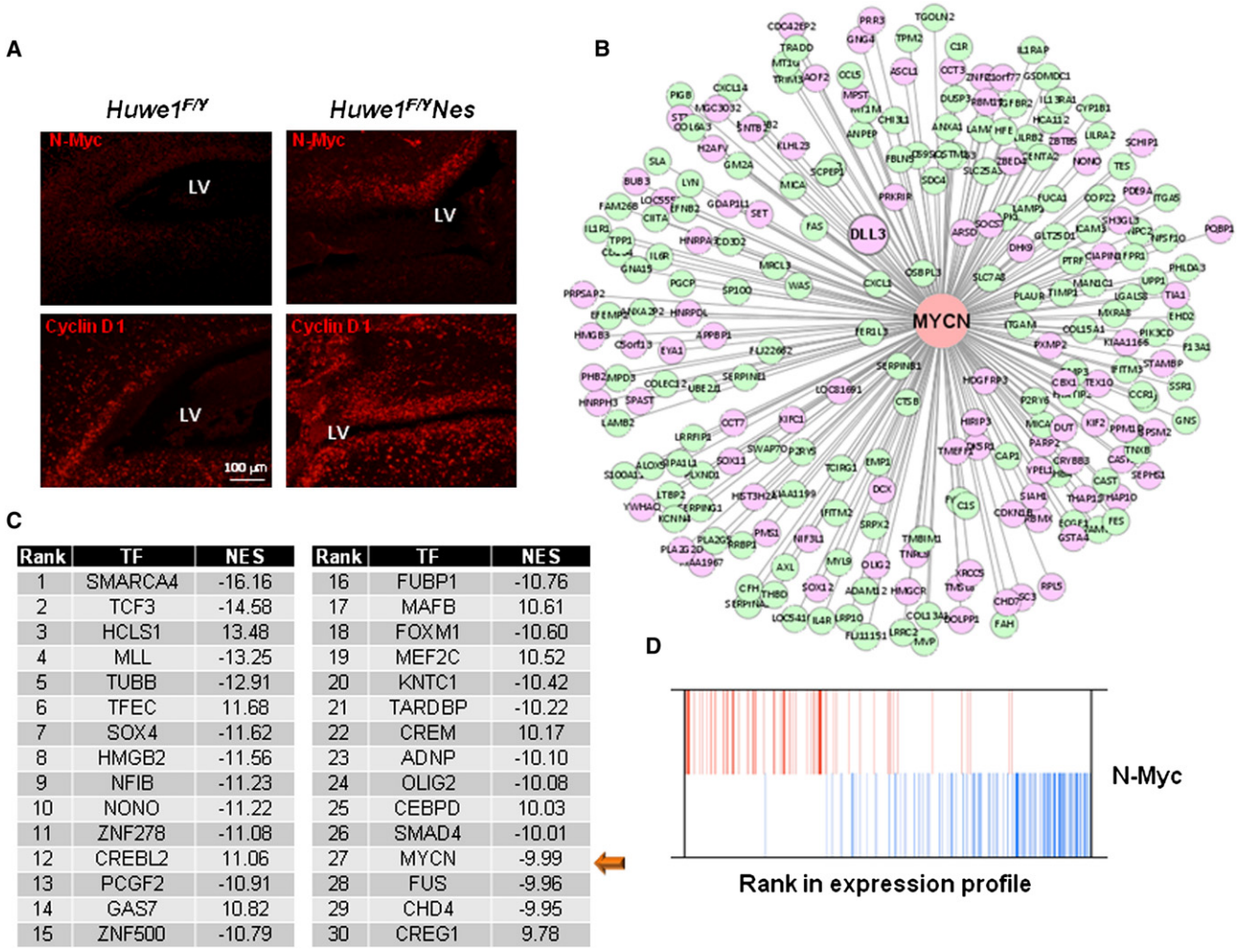

Rank	TF	NES	Rank	TF	NES
1	SMARCA4	-16.16	16	FUBP1	-10.76
2	TCF3	-14.58	17	MAFB	10.61
3	HCLS1	13.48	18	FOXM1	-10.60
4	MLL	-13.25	19	MEF2C	10.52
5	TUBB	-12.91	20	KNTC1	-10.42
6	TFEC	11.68	21	TARDBP	-10.22
7	SOX4	-11.62	22	CREM	10.17
8	HMGB2	-11.56	23	ADNP	-10.10
9	NFIB	-11.23	24	OLIG2	-10.08
10	NONO	-11.22	25	CEBPD	10.03
11	ZNF278	-11.08	26	SMAD4	-10.01
12	CREBL2	11.06	27	MYCN	-9.99
13	PCGF2	-10.91	28	FUS	-9.96
14	GAS7	10.82	29	CHD4	-9.95
15	ZNF500	-10.79	30	CREG1	9.78

Figure 3. *Huwe1* Negatively Regulates the Accumulation and Activity of N-Myc

(A) E18.5 cortical sections were stained for N-Myc (upper panel) and cyclin D1 (lower panels). LV, lateral ventricle.

(B) The N-Myc subnetwork in GBM. Positively and negatively connected genes are shown in pink and green, respectively.

(C) Ranking of the top 30 transcription factors showing changes in their regulon expression based on the Huwe1 expression status in 236 human GBM. Positive and negative normalized enrichment score (NES) values indicate positive and negative association (respectively) of the transcription factor's activities with the expression of *Huwe1*.

(D) GSEA[2] plot for N-Myc regulon genes. All genes are sorted on the horizontal axis according to their differential expression between two extreme expression states of Huwe1, with the most downregulated gene on the left and the most upregulated gene on the right. Red/blue bars indicate overlaps between the ranked list and the individual positive/negative N-Myc targets ($p < 1 \times 10^{-5}$).

but it was notably elevated in the absence of *Huwe1* (Figure 3A, lower panels, and Figure S7B, lower panels). Although elevation of cyclin D1 (and downregulation of $p27^{Kip2}$, Figure S7C) may explain some of the events elicited by deregulated N-Myc in the *Huwe1* knockout cortex, Myc transcription factors display remarkable cell-type specificity for target activation (Eilers and Eisenman, 2008). To unravel the complement of N-Myc transcriptional targets (regulon) in the nervous system, we developed a screen for N-Myc target genes based on a reverse engineering approach. This analysis was performed on 176 malignant glioma samples that had been analyzed by global gene expression profiling (Phillips et al., 2006; Freije et al, 2004; Nigro et al., 2005), and the ARACNe algorithm (*algorithm for the reconstruction of accurate cellular networks*) was used to infer a global transcriptional network (Basso et al., 2005). N-Myc, but not c-Myc, emerged among the 10% largest transcriptional hubs, displaying an inferred subnetwork of 230 highly significant inferred targets ($p < 0.005$, Bonferroni corrected), among which 88 are positively regulated and 142 repressed by N-Myc (Figure 3B and Table S2). Having identified a neural-specific set of N-Myc-regulated target genes (the N-Myc regulon), we interrogated the expression profile tumor data set—236 glioblastoma (GBM) samples—from The Cancer Genome Atlas (TCGA) project to determine whether the N-Myc regulon is differentially regulated in tumor sample subsets where *Huwe1* is differentially expressed (i.e., low expression in one subset and high expression in the other). The two subsets were generated by sorting all glioma samples by *Huwe1* expression and then by selecting

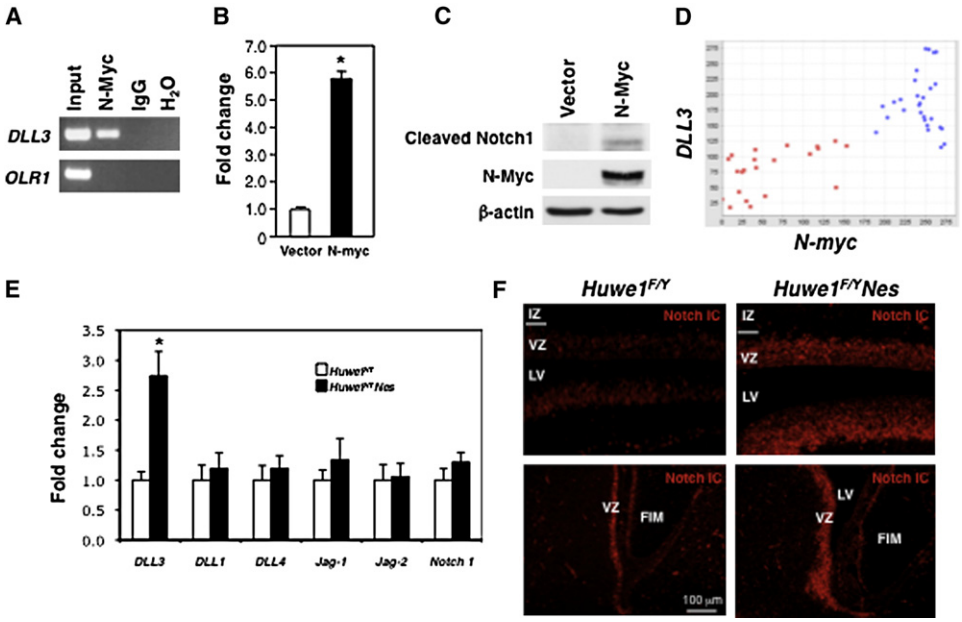

Figure 4. Loss of Huwe1 Activates Notch

(A) Chromatin immunoprecipitation shows that the N-Myc protein binds the promoter of *DLL3*, but not *OLR1*, in neuroblastoma cells.

(B) Quantitative RT-PCR for *DLL3* after ectopic expression of N-Myc in mouse embryo fibroblasts (MEFs). Values were normalized for *β-actin*. Bars indicate mean ± SD of triplicate samples, $p = 4.5 \times 10^{-6}$.

(C) Western blot for cleaved Notch1, N-Myc, and β-actin.

(D) Correlation of the expression of *N-myc* and *DLL3* in human GBM cells cultured in NBE (blue dots) and serum (red dots).

(E) RNA was prepared from E18.5 and P0 brains and analyzed by quantitative RT-PCR for the indicated genes. Values are normalized for *β-actin*. Bars indicate mean ± SD; n = 6 for *Huwe1*^{FY} and 6 for *Huwe1*$^{F/Y}$*Nes*; p = 0.00027 for *DLL3*.

(F) Brain sections from E15.5 (upper panels) and E18.5 (lower panels) embryos were stained for cleaved Notch1.

the first and last 83 (35%) samples. Differential regulation of the N-Myc regulon was assessed using an extension of the Gene Set Enrichment Analysis (GSEA) method (Subramanian et al., 2005), called GSEA^2, developed to simultaneously analyze the enrichment of both activated and repressed targets of a transcription factor (see Experimental Procedures and Lim et al., 2009). When a Gene Ontology (GO) database-derived list of over 1000 transcription factors was tested for differential activity on their regulon, conditional on *Huwe1* expression, N-Myc was ranked among the top 30 (Figure 3C). The analysis of the GSEA^2 plot revealed marked loss of N-Myc transcriptional activity in tumors with high *Huwe1* expression, i.e., concurrent downregulation of N-Myc-activated targets and upregulation of N-Myc-repressed targets ($p < 1 \times 10^{-5}$, Figure 3D). We also asked whether Huwe1 controls the activity of c-Myc. The GBM-derived regulon of c-Myc was noticeably smaller than that of N-Myc (97 versus 230 inferred targets, Figure S8A and Table S3). The GSEA^2 plot showed that the c-Myc regulon was similarly inactivated in tumors with high Huwe1 expression (Figure S8B). Taken together, the computational results indicate that Huwe1 operates as repressor of N-Myc and c-Myc transcription in neural tissue.

Recruitment of Active Notch Signaling by N-Myc Protein Accumulation in Huwe1 Knockout Brain

One of the highest-confidence N-Myc-positive targets inferred by ARACNe is the Notch ligand *DLL3* (Figure 3B). Active Notch signaling is required to maintain neural cells in a multipotent, proliferative state and to inhibit differentiation (Hitoshi et al., 2002; Mizutani et al., 2007; Nagao et al., 2007; Yoon and Gaiano, 2005). Therefore, we asked whether (1) *DLL3* could be validated as a direct N-Myc target gene; (2) N-Myc activates Notch signaling; (3) DLL3 is overexpressed in *Huwe1* knockout brain, and (4) Notch signaling is activated in *Huwe1* knockout brain. The regulatory DNA region adjacent to the *DLL3* gene contained N-Myc-binding sites (E-boxes), and chromatin immunoprecipitation from *N-myc*-amplified neuroblastoma cells demonstrated that endogenous N-Myc is physically associated with the *DLL3* promoter but not irrelevant genomic DNA sequences (Figure 4A). Furthermore, ectopic expression of N-Myc induced the expression of *DLL3* (Figure 4B) and Notch1 activation, as measured by western blot analysis for the cleaved and activated intracellular form of Notch1 (Notch1-IC, Figure 4C). When similar amounts of N-Myc and c-Myc were expressed in the same cells, N-Myc, but not c-Myc, induced the expression of *DLL3* mRNA and DLL3 protein (Figures S9A and S9C). However, c-Myc induced efficiently the expression of two classical Myc-target genes (*ODC* and *cdc25A*), indicating that the inability of c-Myc to induce *DLL3* was not consequent to a generally lower transcriptional activity by c-Myc (Figure S9A). Accordingly, N-Myc, but not c-Myc, induced cleaved Notch1 (Figure S9B). The ability of N-Myc, but not c-Myc, to induce *DLL3* is consistent with the presence of *DLL3* in the regulon of N-Myc, but not c-Myc (Figures 3B and S8A and Tables S2 and S3). To provide further validation for the N-Myc-DLL3 axis, we asked whether expression of *N-myc* and *DLL3* were concurrently regulated in neural cells

retaining stem cell features as opposed to the same cells growing under conditions characterized by rapid loss of stemness. GBM cultures grown in serum-free Neurobasal medium containing EGF and basic FGF (NBE) are similar to normal neural stem cells whereas switching these cells to serum-containing culture conditions leads to rapid loss of their stemness (Lee et al., 2006). By using an entirely independent brain tumor data set, a recent report compared the gene expression profile of NBE-growing brain tumor stem cells with that from the same cells growing in serum (Lee et al., 2006). Gene expression profile data confirmed that *N-myc* and *DLL3* are strongly coregulated in this alternative data set. Additionally, the two genes were shown to be abundantly expressed in NBE-growing brain tumor stem cells but significantly and concurrently depleted in the serum-growing counterparts (Figure 4D).

Next, we asked whether the elevated levels of N-Myc detected in the *Huwe1* null brain increased *DLL3* expression and activated Notch signaling. Quantitative RT-PCR expression analysis for the Notch ligands *DLL1*, *DLL3*, *DLL4*, *Jagged-1*, and *Jagged-2* and the *Notch1* gene revealed that *DLL3* mRNA was the only component of the Notch pathway elevated in *Huwe1* null brain at every developmental stage (Figures 4E and S9D). Furthermore, immunostaining of *Huwe1* knockout and wild-type brains for Notch1-IC revealed a marked increase in the absence of *Huwe1* at E15.5 (Figure 4F, upper panels) and E18.5 (Figure 4F, lower panels). Notably, the Notch1-IC-positive domain overlapped with the region showing the highest expression of the N-Myc protein. Taken together, these findings suggest that an N-Myc-DLL3 cascade may be a key functional target of Huwe1 during neural development.

N-Myc and DLL3 Are Responsible for the Defects in the *Huwe1* Null Brain

To explore the functional significance of the activation of the N-Myc-DLL3 axis for the abnormalities of the *Huwe1* knockout cortex, we analyzed the consequences of silencing *N-myc* or *DLL3* in *Huwe1* null brains. Electroporation of a Cre-GFP-expressing plasmid in the cortical germinal layers of $Huwe1^{Flox}$ embryos produced efficient recombination of the floxed allele (Figure S10). We analyzed BrdU incorporation and performed immunostaining for the neuronal differentiation marker TuJ1 and the DLL3 protein in sections obtained from organotypic slice cultures derived from electroporated E14.5 $Huwe1^{Flox}$ brains (Hand et al., 2005; Nguyen et al., 2006). Compared to GFP-electroporated cortices, electroporation of Cre-GFP triggered the same abnormalities detected in $Huwe1^{F/Y}Nes$ brains (increased proliferation, impaired neuronal differentiation, and overexpression of DLL3, Figures 5A–5C). Expression of Cre-GFP in the presence of specific siRNA oligonucleotides targeting *N-myc* or *DLL3*, but not control siRNAs, rescued the hyperproliferation and the differentiation defects caused by *Huwe1* inactivation (Figures 5A and 5B). Interestingly, the expression of DLL3 was reversed in *Huwe1* null cells electroporated with *N-myc* siRNA oligonucleotides, indicating that loss of Huwe1 triggers elevation of DLL3 through N-Myc (Figure 5C). Thus, the defects generated by inactivation of *Huwe1* require an active N-Myc-DLL3 pathway.

To test whether ectopic expression of Huwe1 in the developing normal brain produces phenotypic and molecular effects that complement those elicited by loss of *Huwe1*, we electroporated embryo cortices with V5-tagged Huwe1 wild-type plasmids expressing the 500 kD full-length Huwe1 protein (*V5-Huwe1*) or the catalytically inactive C4341A point mutant (*V5-Huwe1-CA*). Expression of V5-Huwe1 wild-type, but not V5-Huwe1-CA mutant, caused dramatic inhibition of cell cycle progression and significantly reduced expression of DLL3 (Figures 6A and 6B). Taken together, these data suggest that Huwe1 controls the timing of cell cycle withdrawal and initiation of differentiation in the developing brain by eliminating the N-Myc-DLL3 cascade from cortical progenitors.

The Huwe1-N-Myc Pathway Is Targeted by Genetic and Epigenetic Alterations in Malignant Brain Tumors

It has been proposed that human brain tumors are initiated and maintained by alterations in pathways that regulate self-renewal and differentiation of neural stem cells (Rich and Eyler, 2008; Stiles and Rowitch, 2008; Sutter et al., 2007). Given the importance of the Huwe1-N-Myc pathway in the biology of neural stem cells and neurogenesis in vivo, we asked whether the genes encoding *N-myc* and *Huwe1* are targeted by alterations in human brain tumors. GBM is a CNS tumor for which the most likely cells of origin are neural stem cells. TCGA provides data on the DNA copy number of primary GBM samples (TCGARN, 2008). We interrogated the high-density Affymetrix 6.0 platform of SNPs arrays in the Atlas tumor collection for the possible occurrence of genetic alterations in the *N-myc* and *Huwe1* loci by using the Partek Genomics Suite 6.08. Eight of one hundred and twenty-nine (or six point two percent) tumors carry amplification of the *N-myc* gene. Remarkably, we discovered that two of the eight *N-myc*-amplified tumors (25%), but none of the tumors lacking *N-myc* gene amplification, contain focal deletions of the *Huwe1* gene (FET p = 0.0034, Figure 7A). Detailed mapping of the breakpoints revealed that both deletions remove a minimal region including coding exons 2–20 of *Huwe1* but do not affect the neighboring genetic loci (80 marker probes are deleted in tumor #178 and 31 marker probes are deleted in tumor #289, Figure 7B). Interestingly, *Huwe1* is located on the X chromosome (Xp11.22) and both of the two patients whose tumors contain deletion of *Huwe1* are males (XY). Therefore, the two tumors are converted to a *Huwe1* null state in a manner functionally analogous to that of other tumor suppressor genes that undergo complete loss of function in glioma (e.g., *Ink4a*, *PTEN*) (TCGARN, 2008). Next, we asked whether loss of *Huwe1* expression is also associated with brain tumorigenesis. To this end, we used the ONCOMINE database (www.oncomine.com), which contains gene expression data compiled from the microarray analysis of 23 nontumor human brain samples compared to 77 GBM samples. Interestingly, the GBM samples showed a highly significant ($p = 9.3x10^{-10}$) downregulation of *Huwe1* mRNA in comparison to the corresponding brain tissues (Figure 7C). Thus, malignant brain tumors inactivate the *Huwe1* gene through both genetic and epigenetic alterations.

DISCUSSION

Restriction of self-renewal and proliferation of neural stem cells are coupled to neurogenesis to coordinate cortical architecture during development. In this study, we have conditionally deleted

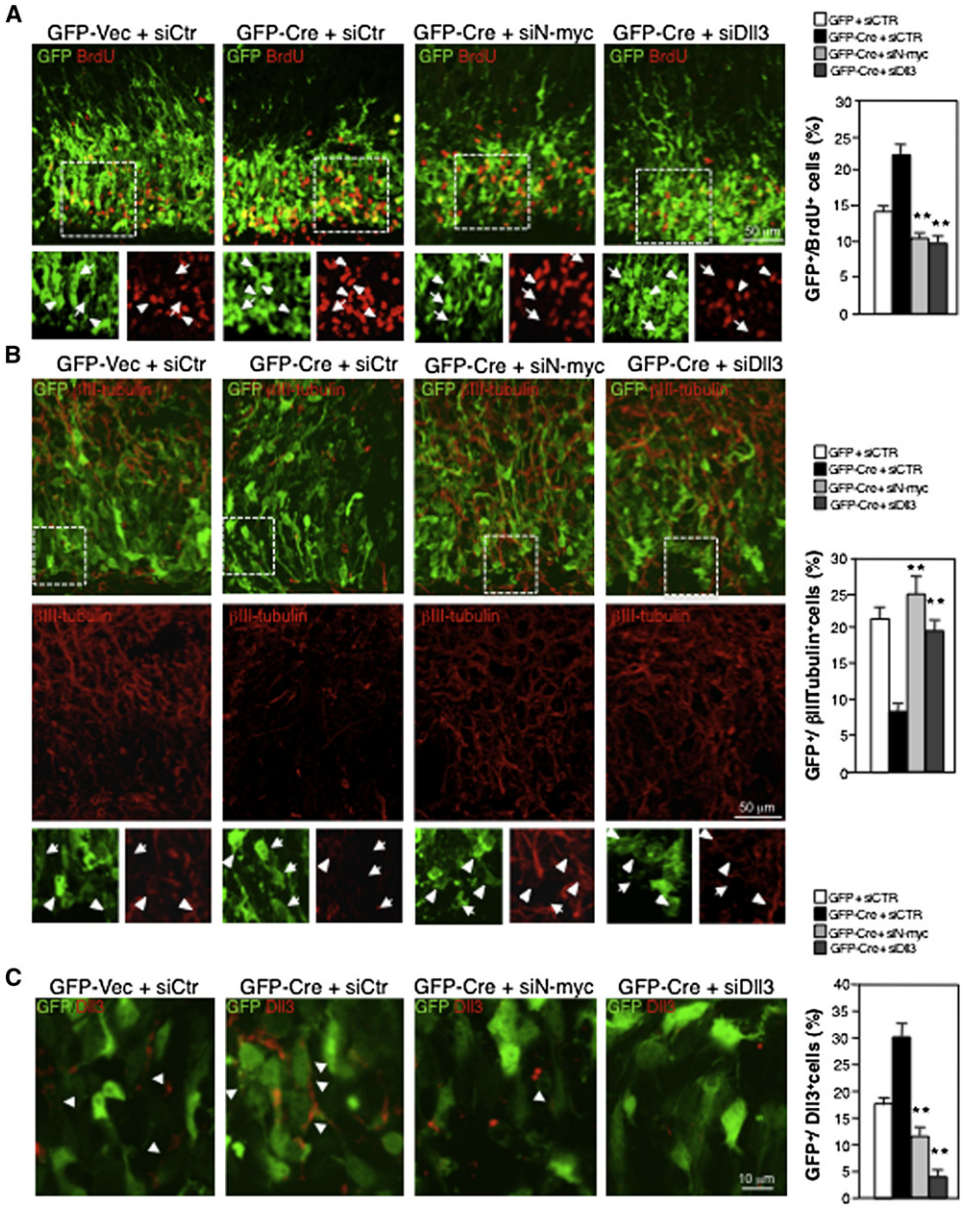

Figure 5. The Huwe1-N-Myc-DLL3 Pathway in the Developing Brain

(A) Ex vivo electroporation of MSCV-GFP or MSCV-GFP-Cre plasmid together with control, *N-myc*, or *Dll3* siRNA into E14.5 mouse cortices followed by organotypic slice culture for 2 days. Cortical sections were stained for GFP (green) and BrdU (red). Arrowheads indicate GFP$^+$/BrdU$^+$ cells; arrows indicate GFP$^+$/BrdU$^-$ cells.

(B) Cortical slices were stained with the neuronal marker βIII-tubulin (red) and GFP (green). Arrowheads indicate GFP$^+$/βIII-tubulin$^+$ cells; arrows indicate GFP$^+$/βIII-tubulin$^-$ cells.

(C) Immunofluorescence with GFP (green) and DLL3 (red) antibodies. Arrowheads indicate GFP$^+$/DLL3$^+$ cells. Double positive cells were scored and quantitative results are shown as mean ± SD from at least three electroporated embryos per group from a minimum of two experiments. **$p < 0.01$, Student's t test.

the *Huwe1* gene in the mouse brain and demonstrated that this enzyme is essential for the transition from self-renewing and proliferating neural stem/progenitor cells to differentiated neurons. Consequently, loss of *Huwe1* severely perturbs neurogenesis and leads to disorganization of the laminar structure of the cortex. We have identified the "N-Myc-DLL3" pathway as mediator of the abnormalities detected in *Huwe1* null brain. The identification of this pathway is the missing link between two crucial transcriptional regulators that provide essential signals for neural stem cell activity and inhibition of neuronal differentiation. Interestingly, a recent study reported loss of Notch activation in the mouse cortex by neural-specific mutation of another E3 ubiquitin ligase, Mind Bomb 1 (Yoon et al., 2008). Together, we suggest that neural development requires a fine balance of ubiquitin ligases with positive (Mind Bomb 1) and negative (Huwe1) signaling ability converging on the Notch pathway. Our work also identifies focal intragenic deletions of the *Huwe1* gene in GBM, a human brain tumor sustained by deregulated neural-stem

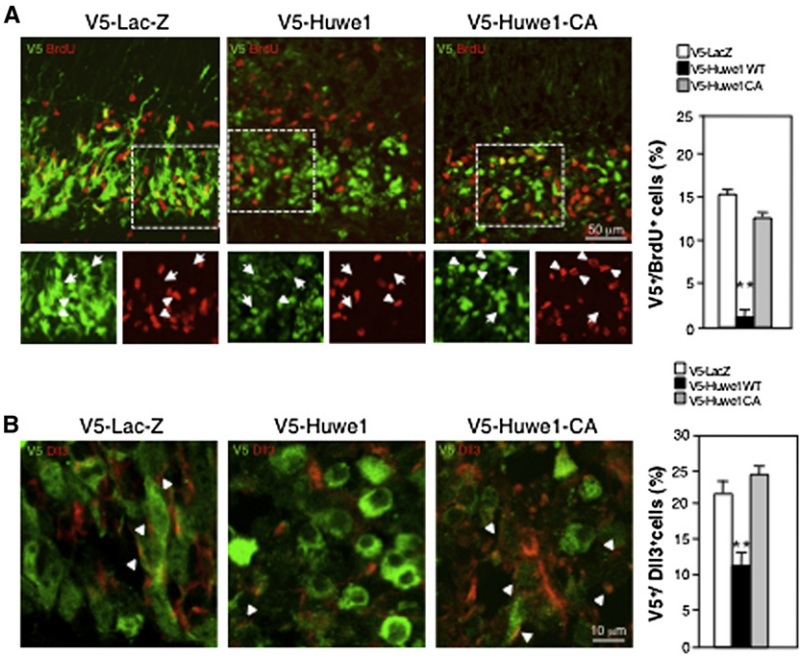

Figure 6. Ectopic Expression of Huwe1 Inhibits Proliferation and Impairs Expression of DLL3

(A) Ex vivo electroporation of pcDNA3.1/V5-His/LacZ, pcDNA3.1/V5-Huwe1-WT, and pcDNA3.1/V5-Huwe1-CA plasmid into E14.5 mouse cortices followed by organotypic slice culture for 2 days. Cortical sections were double-stained with V5 (green) and BrdU (red). Arrowheads indicate $V5^+/BrdU^+$ cells; arrows indicate $V5^+/BrdU^-$ cells.

(B) Cortical sections were stained with V5 (green) and DLL3 (red). Arrowheads indicate $V5^+/DLL3^+$ cells. Double positive cells were scored and quantitative results are shown as mean ± SD from at least three electroporated embryos per group from a minimum of two experiments. $^{**}p < 0.01$.

like activity and marked anaplasia. Thus, mutations of a ubiquitin ligase that restrains proliferation, initiates neurogenesis, and organizes the laminar patterning of the cortex are selected during oncogenic transformation in the human brain.

Huwe1 Restrains Proliferation and Initiates Neurogenesis by Suppressing an N-Myc-DLL3 Cascade in the Developing Brain

The expansion of the neural stem cell compartment elicited by loss of *Huwe1* becomes progressively more evident as neural development proceeds and *Huwe1*$^{-/-}$ neural stem/progenitor cells fail to exit cell cycle and commence neuronal differentiation. The deregulated proliferative activity conferred by loss of *Huwe1* together with abnormal cell morphology and loss of "crowd control" ultimately lead to severe perturbation of neuronal differentiation and disorganization of brain architecture (Dehay and Kennedy, 2007). During relatively early stages of neurogenesis (before E14.5), cell cycle timing is not affected by mutation of *Huwe1*. However, loss of Huwe1 severely impairs the lengthening of the cell cycle that accompanies the progressive shift from proliferation to differentiation during late neurogenesis.

The phenotype of the Huwe1 mutant brain in the mouse is complementary to that caused by inactivation of transcription factors that expand the neural stem cell compartment and inhibit neurogenesis (N-Myc and Notch) (Hitoshi et al., 2002; Knoepfler et al., 2002; Mizutani et al., 2007). We found that the N-Myc protein markedly accumulated in the *Huwe1* null brain and that this effect preceded the phenotypic defects. To unravel the identity of the downstream signaling events triggered by aberrant N-Myc in *Huwe1* null brain, we designed a computational approach to dissect and interrogate the activity of transcription factors following modulation of candidate regulators in a specific cellular context. From this approach, the Notch ligand DLL3 emerged as one of the strongest inferred N-Myc targets in the brain, and we have confirmed that, during neural development, Huwe1 negatively regulates expression of DLL3 in an N-Myc-dependent fashion. Based on this information, we have experimentally validated *DLL3* as a direct transcriptional target of N-Myc and, most importantly, we discovered that the hyperproliferation and neuronal differentiation defects resulting from knocking out *Huwe1* in the cortex are fully reversed by silencing the expression of *DLL3* in vivo. Thus, the N-Myc-DLL3 cascade is restrained by Huwe1 to set the timing of cell cycle withdrawal and neuronal differentiation in the developing brain. Although our results are consistent with DLL3 activating Notch1 in the neural stem cell compartment at midgestation, in other systems DLL3 might also behave as inhibitor of Notch1, possibly through competition with other Notch ligands (Geffers et al., 2007; Ladi et al., 2005).

Huwe1 as Tumor Suppressor Gene in GBM

Activation of stem cell activity and deregulation of N-Myc (and Notch) have been linked to tumorigenesis in the brain (Stiles and Rowitch, 2008; Sutter et al., 2007). High-density gene copy number analysis discovered that at least two tumors (both of which originated in male patients) had highly focal deletions that were entirely contained within the coding region of the *Huwe1* gene. The reduced expression of *Huwe1* in GBM suggests that epigenetic alterations may be more frequently involved. Thus, *Huwe1* resembles the X-linked tumor suppressor *WTX* gene, for which inactivation of the single allele in tumor-bearing male patients is sufficient to create a complete loss-of-function status in tumor cells (Rivera et al., 2007). The *Huwe1* mutations display an additional feature in that they coexist with *N-myc* gene amplification in GBM. Although the finalistic concurrence of *N-myc* and *Huwe1* alterations in the same tumors may seem counterintuitive, cooperation between two independent genetic events is consistent with the mechanisms leading to activation of c-Myc in Burkitt's and other lymphomas, in which transcriptional deregulation of the *c-myc* gene requires translocation to the immunoglobulin loci and is associated with escape from ubiquitin-mediated degradation by the c-Myc protein through independent mutation of regulatory phosphorylation sites (Bahram et al., 2000; Bhatia et al., 1993). Thus, the short half-life of the N-Myc protein in neural cells requires that the increasingly synthesized protein in brain tumors be stabilized

A

	MYCN			HUWE1		
Sample ID	Amplification start	Amplification end	P-value	Deletion start	Deletion end	P-value
178	2784	18069687	0	53608116	53794420	8.91E-09
289	15467044	16299362	3.83E-15	53659906	53724995	2.05E-05
1	4635081	24442762	0			
113	13471051	25094074	0			
133	13569503	31688245	8.14E-16			
221	4296721	22154052	0			
258	14623613	16725987	0			
517	9867746	24450636	0			

B

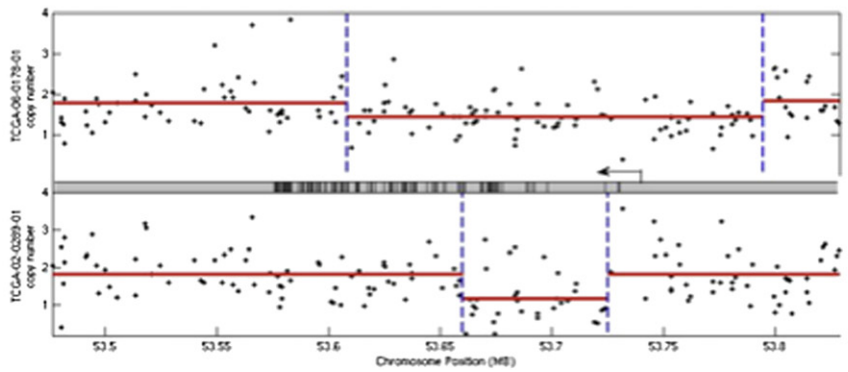

C

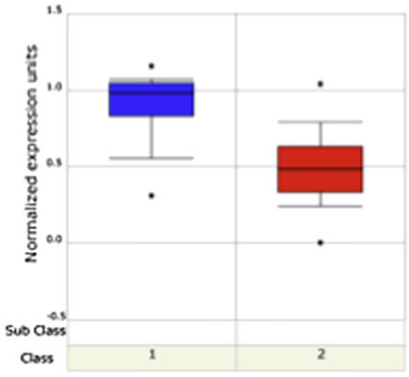

Figure 7. Hemizygous Focal Deletions Target *Huwe1* in GBM

(A) Eight of one hundred twenty-nine GBM contain amplification of the *N-myc* gene, and two of them (#178 and #289) have focal deletions of *Huwe1*.

(B) The two *Huwe1* deletions occur in male (XY) patients and define a focal minimal common region of deletion of 65 kb, which is entirely contained within the *Huwe1* gene. The blue, dashed lines define the limits of the deletions for each tumor.

(C) The expression of Huwe1 is significantly downregulated in 77 samples from human GBM (class 2, red) compared with 23 samples from nontumor human brain (class 1, blue); $p = 9.3x10^{-10}$. Boxes, interquartile range of expression values. The whiskers extend to the 5th and 95th percentile of expression values.

by independent genetic loss of the gene encoding for the ubiquitin ligase Huwe1. We predict that neural stem cells carrying concurrent deletion of *Huwe1* and transcriptional activation of the *N-myc* oncogene gain the most powerful myc-associated activities necessary for oncogenic transformation.

EXPERIMENTAL PROCEDURES

Generation of *Huwe1^{Flox} Nes* Mice

To generate *Huwe1$^{F/Y}$Nes* animals, heterozygous or homozygous floxed *Huwe1* females (*Huwe1$^{Flox/X}$* or *Huwe1$^{Flox/Flox}$*) were bred onto *Nestin-Cre* heterozygous males. *Huwe1* mutants were genotyped by PCR of genomic DNA prepared from tail biopsies using primers described previously (Zhao et al., 2008). All animal experiments were approved by and performed in accordance with the guidelines of the International Agency for Research on Cancer's Animal Care and Use Committee.

Tissue Preparation for Paraffin-Embedded Sections and Immunostaining

Short pulse BrdU (Sigma-Aldrich) labeling was carried out by injecting pregnant mice with BrdU intraperitoneally (50 μg/g body weight) 1 hr prior to sacrifice. For birthdating experiments, timed-pregnant mice (at E12.5 and E15.5) were injected with BrdU intraperitoneally at 40 μg/g body weight. PFA-perfused embryos (E13.5 and E15.5) or dissected brains (E18.5 and P0) were fixed for 24 hr in 10% formalin. Five-micron paraffin sections were deparaffinized, rehydrated, treated for antigen retrieval, and incubated in 10% serum blocking solution prior to the incubation with primary antibodies at room temperature (RT) for 1 hr or at 4°C for 18 hr. For BrdU staining, sections were treated with 3N HCl for 50 min at RT followed by two rinses of 0.1 M boric acid (pH 8.0) for 5 min at RT prior to blocking. Fluorescent detection was performed with Cy3 or FITC-labeled secondary antibodies (Jackson Immunoresearch Laboratories), whereas biotin-conjugated secondary antibodies (Vector Laboratories) were employed for Vectastain Elite ABC development. Tyramide amplification system (Perkin Elmer) was used for Notch-IC, N-Myc, and cyclin D1 immunodetection according to the manufacturer's instructions. The primary antibodies used were as follows: anti-cleaved Notch1 (Val1744, Cell Signaling Technology); anti-BrdU (Roche); anti-Ki67 (Novocastra); anti-Ctip2 (Abcam); anti-MAP2 (Sigma); anti-GAP43, anti-cyclin D1, and anti-HuC/D (Invitrogen); anti-N-Myc (Calbiochem); anti-HUWE1 HECT-domain (Lifespan Biosciences); anti-HUWE1-Lasu1 (Bethyl Laboratories); anti-p27 (Thermo Scientific); anti-Tbr1, anti-Tbr2, anti-Reelin, and anti-Pax6 (Millipore); and anti-Cux1 (Santa Cruz).

Ex Vivo Electroporation and Immunostaining on Cryosections

Ex vivo electroporation was performed as described previously with minor modifications (Zhao et al., 2008). Huwe1 floxed embryos were recovered at E14.5. Endotoxin-free GFP plasmid (1 μg/μl, MSCV-GFP or MSCV-Cre-GFP) mixed with siRNA (10 μM, N-myc, DLL3, and Control Smart Pool, Dharmacon) were injected into lateral ventricles using a Femtojet microinjector (Eppendorf). In Huwe1 overexpression experiments, pcDNA3.1/V5-His/LacZ, pcDNA3.1/V5-Huwe1-WT or pcDNA3.1/V5-Huwe1-CA plasmids (2 μg/μl) were used for electroporation. Electroporated cerebral hemispheres were dissected and sectioned coronally into 300 μm thick slices using a vibratome (VT1000S, Leica). The slices were cultured for 2 days in neurobasal medium containing 1% N2, 1% B27, 2 mM L-glutamine, penicillin-streptomycin, and fungizone. Medium was changed every day. Slices were labeled with 10 μM BrdU for 2 hr followed by fixation in ice-cold 4% PFA at 4°C for 20 hr. Fixed slices were incubated for 24 hr in PBS containing 15% sucrose followed by 24 hr incubation in PBS with 30% sucrose and embedded in optimal cutting

temperature compound (OCT). For each staining, 10 μm sections of at least three brains per group from two independent experiments were used. The antibodies used for double staining on cryosections were as follows: Brdu (Roche), anti-Brdu (Abcam), anti-V5 (Invitrogen), anti-βIII-tubulin (Promega), anti-DLL3 (Santa Cruz), and anti-GFP (Invitrogen). Confocal images acquired with a Zeiss Axioscop2 FS MOT microscope were used to score double positive.

Statistical Analysis

Each experiment was performed with samples from at least three animals from two independent litters. In histograms, values represent the mean values; error bars are standard deviations. Statistical significance was determined by t test (with Welch's Correction) using GraphPad Prism 4.0 software (GraphPad Inc., San Diego, CA).

ARACNe

ARACNe employs an information theoretic approach to infer transcriptional interactions by considering statistical dependencies between the gene expression profiles (Basso et al., 2005). The algorithm first distinguishes candidate interactions between a transcription factor and its potential target by computing pairwise mutual information (MI) taking advantage of a computationally efficient Gaussian Kernel estimator. The algorithm then eliminates the vast majority of interactions that are likely mediated by another transcription factor using the Data Processing Inequality (DPI) theorem. The procedure is repeated for 100 times to generate a set of bootstrap networks with pseudo data sets randomly sampled (with replacement) from the original data set. Finally, a consensus network is constructed by retaining interactions supported across a significant number of the bootstrap networks. In contrast to coexpression networks, ARACNe explicitly discriminates between direct and indirect transcriptional interactions, an essential feature in reducing false positives among the inferred targets of a transcription factor. In transcriptional networks it has been shown that a small percent of genes accounts for most of the interaction; the transcription factors with the largest number of regulated targets in the network are called hubs (Barabasi and Oltvai, 2004; Zhu et al., 2007).

GSEA^2

Microarray samples were first partitioned into two 35% subsets where Huwe1 is relatively most and least expressed. GSEA^2 was used to assess whether transcriptional targets of a transcription factor are statistically enriched in genes differentially expressed between the two subsets. The algorithm considers differential expressions of a transcription factor's positive and negative targets as the reflection of changes in the transcription factor's activity. Supposing that activity of a transcription factor is negatively associated with the abundance of Huwe1 (e.g., Huwe1 ubiquitinates and degrades a transcription factor), one would expect the transcription-factor-activated targets to be enriched in genes that are downregulated, whereas the transcription-factor-repressed targets would be enriched in genes that are upregulated when Huwe1 is highly expressed. Statistical significance of the enrichment is then determined by comparing the observed enrichment score to the null distribution computed through random permutation of the transcriptional target sets. Details of the algorithm have been previously described in Lim et al. (2009).

Promoter Analysis and Chromatin Immunoprecipitation

Promoter analysis was performed using MatInspector software (www.genomatix.de). A sequence of 2 kb upstream and 2 kb downstream from the transcription start site was analyzed for the presence of putative E-box sequences. Primers used to amplify sequences surrounding the predicted binding sites were designed using Primer3 software (http://frodo.wi.mit.edu/cgi-bin/primer3/primer3_www.cgi).

Chromatin immunoprecipitation was performed as described in Frank et al. (2001). IMR32 cells were crosslinked with 1% formaldehyde for 10 min and stopped with 0.125 M glycine for 5 min. Cells were washed in PBS and harvested in sodium dodecyl sulfate buffer. After centrifugation, cells were resuspended in ice-cold immunoprecipitation buffer and sonicated to obtain fragments of 500–1000 pb. Lysates were centrifuged at full speed and the supernatant was precleared with Protein A/G beads (Santa Cruz Biotechnology) and incubated at 4°C overnight with 1 μg of polyclonal antibody specific for N-Myc (C-19, Santa Cruz Biotechnology) or 1 μg of normal rabbit immunoglobulins (Santa Cruz Biotechnology). The immunocomplexes were recovered by incubating the lysates with protein A/G for 1 hr at 4°C. After extensive washing the immunocomplexes were eluted and reverse cross-linked, and DNA was recovered by phenol-chloroform extraction and ethanol precipitation. DNA was eluted in 200 μl of water and 1 μl was analyzed by PCR with Platinum Taq (Invitrogen). The sequence of the primers used is listed as follows: DLL3: Forward, AGCGTCACACAATCACGAAG; Reverse, TGGTATGA ACCAGAGCTACCG; OLR: Forward, ACTGCACCTGGCCAACTTTT; Reverse, TGCAAAGAAAAGAATACACAAAGGA.

N-myc and *Huwe1* Gene Copy Number Analysis

Copy number analysis on the TCGA GBM samples was done using Partek Genomics Suite 6.08 (http://www.partek.com/). Both paired and unpaired analysis was done to get the raw copy numbers since some tumor samples did not have corresponding normal samples. To identify regions of amplification and deletion, the genomic segmentation algorithm of Partek was implemented with the following parameters: minimum of ten genomic markers at a p value of 0.001 and a signal-to-noise ratio of 0.3. A p value of 0.01 was used to filter for regions of interest from the segmentation results.

SUPPLEMENTAL DATA

Supplemental data for this article include Supplemental Experimental Procedures, ten figures, and three tables and can be found at http://www.cell.com/developmental-cell/supplemental/S1534-5807(09)00293-7.

ACKNOWLEDGMENTS

This work was supported by grants from the NIH-NCI to A.L. (R01CA131126), A.I. (R01CA085628), and A.C. (R01CA109755); by the National Centers for Biomedical Computing NIH Roadmap initiative (U54CA121852 to A.C.); and by The Chemotherapy Foundation (to A.I.). D.D'A. and M.S.C. are supported by fellowships from Provincia di Benevento/Ministero del Lavoro, Italy.

Received: November 10, 2008
Revised: June 13, 2009
Accepted: July 8, 2009
Published: August 17, 2009

REFERENCES

Adhikary, S., Marinoni, F., Hock, A., Hulleman, E., Popov, N., Beier, R., Bernard, S., Quarto, M., Capra, M., Goettig, S., et al. (2005). The ubiquitin ligase HectH9 regulates transcriptional activation by Myc and is essential for tumor cell proliferation. Cell *123*, 409–421.

Bahram, F., von der Lehr, N., Cetinkaya, C., and Larsson, L.G. (2000). c-Myc hot spot mutations in lymphomas result in inefficient ubiquitination and decreased proteasome-mediated turnover. Blood *95*, 2104–2110.

Barabasi, A.L., and Oltvai, Z.N. (2004). Network biology: understanding the cell's functional organization. Nat. Rev. Genet. *5*, 101–113.

Basso, K., Margolin, A.A., Stolovitzky, G., Klein, U., Dalla-Favera, R., and Califano, A. (2005). Reverse engineering of regulatory networks in human B cells. Nat. Genet. *37*, 382–390.

Bernassola, F., Karin, M., Ciechanover, A., and Melino, G. (2008). The HECT family of E3 ubiquitin ligases: multiple players in cancer development. Cancer Cell *14*, 10–21.

Bhatia, K., Huppi, K., Spangler, G., Siwarski, D., Iyer, R., and Magrath, I. (1993). Point mutations in the c-Myc transactivation domain are common in Burkitt's lymphoma and mouse plasmacytomas. Nat. Genet. *5*, 56–61.

Chen, D., Kon, N., Li, M., Zhang, W., Qin, J., and Gu, W. (2005). ARF-BP1/Mule is a critical mediator of the ARF tumor suppressor. Cell *121*, 1071–1083.

Dehay, C., and Kennedy, H. (2007). Cell-cycle control and cortical development. Nat. Rev. Neurosci. *8*, 438–450.

Doe, C.Q. (2008). Neural stem cells: balancing self-renewal with differentiation. Development *135*, 1575–1587.

Eilers, M., and Eisenman, R.N. (2008). Myc's broad reach. Genes Dev. *22*, 2755–2766.

Ekstrom, P., and Johansson, K. (2003). Differentiation of ganglion cells and amacrine cells in the rat retina: correlation with expression of HuC/D and GAP-43 proteins. Brain Res. Dev. Brain Res. *145*, 1–8.

Englund, C., Fink, A., Lau, C., Pham, D., Daza, R.A., Bulfone, A., Kowalczyk, T., and Hevner, R.F. (2005). Pax6, Tbr2, and Tbr1 are expressed sequentially by radial glia, intermediate progenitor cells, and postmitotic neurons in developing neocortex. J. Neurosci. *25*, 247–251.

Frank, S.R., Schroeder, M., Fernandez, P., Taubert, S., and Amati, B. (2001). Binding of c-Myc to chromatin mediates mitogen-induced acetylation of histone H4 and gene activation. Genes Dev. *15*, 2069–2082.

Freije, W.A., Castro-Vargas, F.E., Fang, Z., Horvath, S., Cloughesy, T., Liau, L.M., Mischel, P.S., Nelson, S.F., et al. (2004). Gene expression profiling of gliomas strongly predicts survival. Cancer Res. *64*, 6503–6510.

Geffers, I., Serth, K., Chapman, G., Jaekel, R., Schuster-Gossler, K., Cordes, R., Sparrow, D.B., Kremmer, E., Dunwoodie, S.L., Klein, T., et al. (2007). Divergent functions and distinct localization of the Notch ligands DLL1 and DLL3 in vivo. J. Cell Biol. *178*, 465–476.

Glickstein, S.B., Alexander, S., and Ross, M.E. (2007). Differences in cyclin D2 and D1 protein expression distinguish forebrain progenitor subsets. Cereb. Cortex *17*, 632–642.

Gotz, M., and Huttner, W.B. (2005). The cell biology of neurogenesis. Nat. Rev. Mol. Cell Biol. *6*, 777–788.

Hall, J.R., Kow, E., Nevis, K.R., Lu, C.K., Luce, K.S., Zhong, Q., and Cook, J.G. (2007). Cdc6 stability is regulated by the Huwe1 ubiquitin ligase after DNA damage. Mol. Biol. Cell *18*, 3340–3350.

Hand, R., Bortone, D., Mattar, P., Nguyen, L., Heng, J.I., Guerrier, S., Boutt, E., Peters, E., Barnes, A.P., Parras, C., et al. (2005). Phosphorylation of Neurogenin2 specifies the migration properties and the dendritic morphology of pyramidal neurons in the neocortex. Neuron *48*, 45–62.

Hitoshi, S., Alexson, T., Tropepe, V., Donoviel, D., Elia, A.J., Nye, J.S., Conlon, R.A., Mak, T.W., Bernstein, A., and van der Kooy, D. (2002). Notch pathway molecules are essential for the maintenance, but not the generation, of mammalian neural stem cells. Genes Dev. *16*, 846–858.

Huang, L., Kinnucan, E., Wang, G., Beaudenon, S., Howley, P.M., Huibregtse, J.M., and Pavletich, N.P. (1999). Structure of an E6AP-UbcH7 complex: insights into ubiquitination by the E2-E3 enzyme cascade. Science *286*, 1321–1326.

Kintner, C. (2002). Neurogenesis in embryos and in adult neural stem cells. J. Neurosci. *22*, 639–643.

Knoepfler, P.S., Cheng, P.F., and Eisenman, R.N. (2002). N-myc is essential during neurogenesis for the rapid expansion of progenitor cell populations and the inhibition of neuronal differentiation. Genes Dev. *16*, 2699–2712.

Ladi, E., Nichols, J.T., Ge, W., Miyamoto, A., Yao, C., Yang, L.T., Boulter, J., Sun, Y.E., Kintner, C., and Weinmaster, G. (2005). The divergent DSL ligand Dll3 does not activate Notch signaling but cell autonomously attenuates signaling induced by other DSL ligands. J. Cell Biol. *170*, 983–992.

Lee, J., Kotliarova, S., Kotliarov, Y., Li, A., Su, Q., Donin, N.M., Pastorino, S., Purow, B.W., Christopher, N., Zhang, W., et al. (2006). Tumor stem cells derived from glioblastomas cultured in bFGF and EGF more closely mirror the phenotype and genotype of primary tumors than do serum-cultured cell lines. Cancer Cell *9*, 391–403.

Lim, W.K., Lyashenko, E., and Califano, A. (2009). Master regulators used as breast cancer metastasis classifier. Pac. Symp. Biocomput. 504–516.

Liu, Z., Oughtred, R., and Wing, S.S. (2005). Characterization of E3Histone, a novel testis ubiquitin protein ligase which ubiquitinates histones. Mol. Cell. Biol. *25*, 2819–2831.

Lothian, C., Prakash, N., Lendahl, U., and Wahlstrom, G.M. (1999). Identification of both general and region-specific embryonic CNS enhancer elements in the nestin promoter. Exp. Cell Res. *248*, 509–519.

Mizutani, K., Yoon, K., Dang, L., Tokunaga, A., and Gaiano, N. (2007). Differential Notch signalling distinguishes neural stem cells from intermediate progenitors. Nature *449*, 351–355.

Nagao, M., Sugimori, M., and Nakafuku, M. (2007). Cross talk between notch and growth factor/cytokine signaling pathways in neural stem cells. Mol. Cell. Biol. *27*, 3982–3994.

Nguyen, L., Besson, A., Heng, J.I., Schuurmans, C., Teboul, L., Parras, C., Philpott, A., Roberts, J.M., and Guillemot, F. (2006). p27kip1 independently promotes neuronal differentiation and migration in the cerebral cortex. Genes Dev. *20*, 1511–1524.

Nigro, J.M., Misra, A., Zhang, L., Smirnov, I., Colman, H., Griffin, C., Ozburn, N., Chen, M., Pan, E., Koul, D., et al. (2005). Integrated array-comparative genomic hybridization and expression array profiles identify clinically relevant molecular subtypes of glioblastoma. Cancer Res. *65*, 1678–1686.

Oliver, T.G., Grasfeder, L.L., Carroll, A.L., Kaiser, C., Gillingham, C.L., Lin, S.M., Wickramasinghe, R., Scott, M.P., and Wechsler-Reya, R.J. (2003). Transcriptional profiling of the Sonic hedgehog response: a critical role for N-myc in proliferation of neuronal precursors. Proc. Natl. Acad. Sci. USA *100*, 7331–7336.

Phillips, H.S., Kharbanda, S., Chen, R., Forrest, W.F., Soriano, R.H., Wu, T.D., Misra, A., Nigro, J.M., Colman, H., Soroceanu, L., Williams, P.M., et al. (2006). Molecular subclasses of high-grade glioma predict prognosis, delineate a pattern of disease progression, and resemble stages in neurogenesis. Cancer Cell *9*, 157–173.

Rich, J.N., and Eyler, C.E. (2008). Cancer stem cells in brain tumor biology. Cold Spring Harb. Symp. Quant. Biol. *73*, 411–420.

Rivera, M.N., Kim, W.J., Wells, J., Driscoll, D.R., Brannigan, B.W., Han, M., Kim, J.C., Feinberg, A.P., Gerald, W.L., Vargas, S.O., et al. (2007). An X chromosome gene, WTX, is commonly inactivated in Wilms tumor. Science *315*, 642–645.

Stiles, C.D., and Rowitch, D.H. (2008). Glioma stem cells: a midterm exam. Neuron *58*, 832–846.

Subramanian, A., Tamayo, P., Mootha, V.K., Mukherjee, S., Ebert, B.L., Gillette, M.A., Paulovich, A., Pomeroy, S.L., Golub, T.R., Lander, E.S., et al. (2005). Gene set enrichment analysis: a knowledge-based approach for interpreting genome-wide expression profiles. Proc. Natl. Acad. Sci. USA *102*, 15545–15550.

Sutter, R., Yadirgi, G., and Marino, S. (2007). Neural stem cells, tumour stem cells and brain tumours: dangerous relationships? Biochim. Biophys. Acta *1776*, 125–137.

Takahashi, T., Nowakowski, R.S., and Caviness, V.S., Jr. (1993). Cell cycle parameters and patterns of nuclear movement in the neocortical proliferative zone of the fetal mouse. J. Neurosci. *13*, 820–833.

Takahashi, T., Nowakowski, R.S., and Caviness, V.S., Jr. (1994). Mode of cell proliferation in the developing mouse neocortex. Proc. Natl. Acad. Sci. USA *91*, 375–379.

Takahashi, T., Nowakowski, R.S., and Caviness, V.S., Jr. (1995a). Early ontogeny of the secondary proliferative population of the embryonic murine cerebral wall. J. Neurosci. *15*, 6058–6068.

Takahashi, T., Nowakowski, R.S., and Caviness, V.S., Jr. (1995b). The cell cycle of the pseudostratified ventricular epithelium of the embryonic murine cerebral wall. J. Neurosci. *15*, 6046–6057.

The Cancer Genome Atlas Research Network (CGARN), (2008). Comprehensive genomic characterization defines human glioblastoma genes and core pathways. Nature *455*, 1061–1068.

Yoon, K., and Gaiano, N. (2005). Notch signaling in the mammalian central nervous system: insights from mouse mutants. Nat. Neurosci. *8*, 709–715.

Yoon, K.J., Koo, B.K., Im, S.K., Jeong, H.W., Ghim, J., Kwon, M.C., Moon, J.S., Miyata, T., and Kong, Y.Y. (2008). Mind bomb 1-expressing intermediate progenitors generate notch signaling to maintain radial glial cells. Neuron *58*, 519–531.

Zhao, X., Heng, J.I., Guardavaccaro, D., Jiang, R., Pagano, M., Guillemot, F., Iavarone, A., and Lasorella, A. (2008). The HECT-domain ubiquitin ligase Huwe1 controls neural differentiation and proliferation by destabilizing the N-Myc oncoprotein. Nat. Cell Biol. *10*, 643–653.

Zhong, Q., Gao, W., Du, F., and Wang, X. (2005). Mule/ARF-BP1, a BH3-only E3 ubiquitin ligase, catalyzes the polyubiquitination of Mcl-1 and regulates apoptosis. Cell *121*, 1085–1095.

Zhu, X., Gerstein, M., and Snyder, M. (2007). Getting connected: analysis and principles of biological networks. Genes Dev. *21*, 1010–1024.